

## **Development of Random and Ordered Composite Fiber Hybrid Technologies for Controlled Release Functions**

**Baolin Wang<sup>1,2,3</sup>, Zeeshan Ahmad<sup>4</sup>, Jie Huang<sup>5</sup>, Jing-song Li<sup>3</sup>, and Ming-Wei Chang<sup>\*1,2,3</sup>,**

<sup>1</sup> College of Biomedical Engineering & Instrument Science, Zhejiang University, Hangzhou, 310027, P.R. China.

<sup>2</sup> Zhejiang Provincial Key Laboratory of Cardio-Cerebral Vascular Detection Technology and Medical Effectiveness Appraisal, Zhejiang University, Hangzhou, 310027, P.R. China.

<sup>3</sup> Key Laboratory for Biomedical Engineering of Education Ministry of China, Zhejiang University, Hangzhou, 310027, P.R. China.

<sup>4</sup> Leicester School of Pharmacy, De Montfort University. The Gateway, Leicester, LE1 9BH, UK.

<sup>5</sup> Department of Mechanical Engineering, University College London, London WC1E7JE, UK.

\*corresponding author: Ming-Wei Chang, Ph.D., Assoc. Professor

Tel: +86(0)571-87951517, Email: mwchang@zju.edu.cn

## **Abstract**

Fibrous technologies (such as membranes, films, patches and filters) and their enabling engineering platforms have gained considerable interest over the last decade. In this study, novel fibrous constructs from a unique engineering platform were developed based on hybrid electrohydrodynamic (EHD) technology; incorporating functional and bioactive materials within random and aligned fibrous formulation geometries. Complex constructs were engineered using 3D printing (polycaprolactone, PCL, for sustained delivery) and electrospinning (polyvinylpyrrolidone, PVP, for rapid release) in an intercalating material layer-by-layer format using a side-by-side technological approach. Here, structure generation proceeded with deposition of ordered PCL fibers enabling well-defined void size and overall dimension, after which randomly spun PVP fibers formed a construct overcoat (as a membrane). Differences between polymer dissolution rate, hydrophilicity, mechanical properties and functional material hosting (and linked external auxiliary magnetic field trigger) provided opportunities to modulate antibiotic drug (tetracycline hydrochloride, TE-HCL) release. In vitro cell studies using human umbilical vein blood vessel cell line demonstrated device biocompatibility and Escherichia Coli (E. coli) was selected to demonstrate anti-bacterial function. Overall, a new hybrid engineering platform to prepare customizable and exciting multi-faceted drug release constructs is elucidated.

**Keywords:** electrospinning; EHD continuous jetting; rapid drug release; sustained drug release; hybrid system.

## **1. Introduction**

Strategies and methods to modulate drug release behaviour have evolved significantly over the last few decades; from polymeric system to nano-functionalized pharmaceuticals [1, 2]. Specifically, a variety of systems have been developed to meet the needs of selected active release behaviour (i.e. immediate, pulsatile, delayed, sustained and biphasic releases [3-5]). Amongst these, sustained drug release systems are currently the most explored; with recent efforts focusing on enhancing drug concentration in blood (within therapeutic window) or target tissues therefore displaying prolonged activity [6, 7]. While this provides a sustained active release period, rapid release features are often neglected, which becomes problematic if an active needs to be delivered immediately, providing a quick biological response.

Electrospinning (ES) has great potential in generating fibrous materials for drug delivery applications [8]. Using such filamentous structure, a host of drugs such as antibiotics and anticancer agents can be delivered [9]. Electrohydrodynamic (EHD) continuous jetting is based on digitally-controlled deposition of materials (often layer by layer) to create well-ordered freeform geometries, unlike random structures obtained when using ES [10]. EHD continuous jetting methods currently deployed in the engineering of pharmaceuticals permit simple, accurate, cheap, structured and tailored developments of drug delivery dosage forms.

Polyvinylpyrrolidone (PVP) is a synthetic, biocompatible and non-toxic polymer which has been widely used as a pharmaceutical excipient (for dosage form development) [11, 12]. Polycaprolactone (PCL) is a hydrophobic polymer with desirable

physicochemical properties, which has been used in diffusion-controlled delivery systems [13].

Fe<sub>3</sub>O<sub>4</sub> nanoparticles (NPs) are rapidly emerging as opportunistic healthcare materials [14]. Recent explorations have shown their potential in cell separation, diagnostics and advanced therapy regimes [15]. In addition, co-encapsulation of Fe<sub>3</sub>O<sub>4</sub> NPs with an active embedded into a polymeric matrix system affords trigger based drug release mechanisms (using an external auxiliary magnetic field (AMF)). In this instance, the functionality of the external trigger is dependent on NP loading within the formulation, strength of the applied field and geometrical features of the drug delivery system [16]. This approach is valuable since it has shown to improve pharmacokinetics of retarded active release systems as and when needed [17].

In recent times multi-step or two tiered drug release systems have gained popularity and these have focused on external triggers, materials and engineering of new and complex structures [18, 19]. However, methods to design and develop such drug delivery systems (combining both rapid and sustained mechanisms) remain limited. To accommodate this several approaches have been undertaken including controlled layering or core-shell structures [20]. Conventional methods (e.g. wet granulation) have also been used to encapsulate or host multiple actives.

In this study, EHD continuous jetting and ES techniques are arranged in a side-by-side hybrid-engineering platform to fabricate mechanically and biologically improved constructs for drug delivery applications through a layer-by-layer materials approach. A non-core shelled delivery system is engineered. In addition to space, process stages

and time benefits the developed system enables greater loading capacity, simultaneous entrapment of therapies where formulations are non-compatible, ease of operation [9] and the ability to alter specific components as required (specific drug and tailored drug loading capability) Multi-layered and well-aligned PCL fibers were used as the construct base (mechanically enforcing) and electrospun PVP membranes provided an overcoat layer. The well-established difference in dissolution and degradation rate between these polymers provided a two-tier active (TE-HCL) release mechanism. TE-HCL, which belongs to a group of broad-spectrum antibiotics and is commonly used to treat and control bacterial skin infections, was used as the model active compound [21-24].

## **2. Materials and methods**

### *2.1 Materials*

Polyvinyl pyrrolidone (PVP,  $M_w = 1.3 \times 10^6$  g/mol) and Poly  $\epsilon$ -caprolactone (PCL, mean  $M_w = 8 \times 10^4$  g/mol) were purchased from Sigma-Aldrich, St Louis, USA. Tetracycline hydrochloride (TE-HCL) was purchased from Amersco, USA.  $Fe_3O_4$  NPs (mean particle diameter~ 20nm) were purchased from HWRK Chem, China. Glacial acetic acid, absolute ethyl alcohol and phosphate buffer saline (PBS, pH 7.4) were supplied by Sinopharm Chemical Reagent, China. All chemicals and reagents were analytical grade.

### *2.2 Solution and suspension preparation*

For EHD continuous jetting, PCL polymer solution (20% w/w) was prepared using acetic acid. To ensure complete dissolution, initial mixtures were mechanically stirred for 5 hrs at the ambient temperature (24 °C). Fe<sub>3</sub>O<sub>4</sub> NPs were incorporated into selected PCL solutions and a second suspension was prepared which hosted both Fe<sub>3</sub>O<sub>4</sub> NPs (0.5 % w/w, of the final composition) and the model active TE-HCL (0.5% w/w, of the final composition). The drug suspension was stirred for 6 hrs to ensure complete dissolution. Both mixtures were placed in mild bath sonication (2 hrs), prior to EHD engineering, which resulted in near homogenous suspensions. TE-HCL release from constructs were evaluated with and without external stimuli (AMF).

A PVP/TE-HCL solution was prepared by adding both drug and polymer to ethyl alcohol at 15 and 0.5% w/w, respectively, (of the overall formulation) followed by mechanical stirring (1 hr). Upon complete dissolution, a known quantity of the solution was magnetized through addition of Fe<sub>3</sub>O<sub>4</sub> NPs (0.5% w/w of the final composition). The mixture was dispersed for 2 hrs by mild bath sonication to ensure a homogenous system.

### *2.3 Complex construct engineering*

A schematic diagram showing the hybrid EHD system (EHD continuous jetting and ES) is shown in Fig. 1. The hybrid system, providing a patterned PCL fiber platform with randomly orientated PVP fibrous mesh overcoat, comprised an X-Y-Z motion stage controlled using mechatronics. This enabled precise programmable movement during construct engineering. Two high-voltage power supplies capable of generating

~30 KV (Glassman high voltage Inc. series FC, USA) were individually connected to EHD continuous jetting and ES nozzles, both of which possessed an inner diameter of 0.5 mm. PCL and PVP/TE-HCL formulations were loaded separately into 5 ml syringes and were subsequently mounted into the precision syringe pumps (KD Scientific KDS100, USA). A conductive glass collector was mounted onto the programmable X-Y-Z motion stage as the ground electrode. The applied voltage for EHD continuous jetting was set in the range 2.0~2.2 kV, and the applied voltage for ES was maintained at 9.0 kV. The deposition distance were set at 5 mm and 6 cm, for EHD continuous jetting and ES, respectively. To maintain a stable cone-jet for the process, solution feed rate for EHD continuous jetting and ES were selected as 0.2 and 0.8ml/h, respectively. Fabrication proceeded by patterning of a 3D PCL based scaffold (first) with precise designated filamentous layers (20 layer overprints). The next step involved the deposition of a PVP membrane comprising randomly oriented fibers *via* ES for 2 mins. All experiments were performed at the ambient temperature (25°C) and relative humidity (40~ 60%).

#### *2.4 Material characterization*

Construct surface morphology was characterized using optical (Phenix BMC503-ICCF, China) and scanning electron microscopy (SEM, FEI Quanta 650, Netherland). For SEM analysis, samples were applied with a thin layer of

platinum for 60 s using a sputter coater (108auto, Cressington Scientific Instruments Ltd., UK) at a current intensity of 25 mA to prevent sample charging. All data was exported for analysis and graphs were plotted using Origin software (OriginLab, USA). Fiber diameters were quantified using a statistical distribution that involved 50 fibers (50 layer overprints) for each experimental condition. Error bars were plotted to represent the mean  $\pm$  standard deviation.

Construct hydrophobicity was assessed using an optical contact angle & interface tension meter (SL2000KB, Kino Industry Co., Ltd, USA). The contact angle of 1 $\mu$ L PBS droplet on selected construct surfaces was measured at pre-determined time intervals. Fourier Transform Infra-Red (FTIR) was used to determine construct composition, interactions and material stability. Samples were prepared using the KBr pellet pressing method. For this, 2 mg of each construct sample was dispersed in 200 mg of KBr medium by grinding and then compressed into transparent pellets (pressure-12 MPa). Pellets were then scanned with FTIR (Ir Affinity 1, Shimadzu, Japan) and acquired spectrum possessed a resolution of 4 cm<sup>-1</sup> (4000-450cm<sup>-1</sup>). Each spectrum was obtained using 20 scans.

In order to investigate pattern impact on construct mechanical properties; tensile tests were performed using a universal materials tester (Zwick/Roell Z020, Zwick, Germany). The selected gauge length was 15 mm, and samples were extended along the fiber axis with a 500 N load cell at a crosshead speed of 10 mm/min at the ambient temperature (24 °C). Construct samples (7  $\times$  2.5 cm) were prepared for tensile tests. For



each sample set, measurements were taken in triplicate after which the mean tensile strength was calculated.

### *2.5 In vitro drug release study*

Drug release was monitored according to a method deployed in a previous study [15]. Assays comprised 10 ml release medium (PBS, pH=7.4) with 30 mg of test sample. Due to the presence of Fe<sub>3</sub>O<sub>4</sub> NPs in some constructs, AMF application impact on drug release from particle hosting constructs was explored. For non-AMF stimulated samples, 2 ml supernatant was removed for UV measurement and replaced with an equal volume of fresh release medium at pre-determined time intervals. Concentration of TE-HCL in supernatant was measured using UV absorption at a wavelength of ~364 nm (UV-2600 spectrophotometer, Shimadzu, Japan).

For AMF related studies, a field was generated around selected vials hosting samples and near identical experiments were conducted without AMF application, serving as the control group. A sinusoidal alternating electric current was generated *via* functional signal generation (AFG1022, Tektronix, USA) and circulated into a copper solenoid after being magnified through a power amplifier (HFVA-42, Foneng Science and Technology Co.,Ltd., Nanjing, China). The AMF was delivered at a fixed operating frequency of 40 kHz and the output current was maintained at 0.4A (induced magnetic strength of 1.5 mT). All experiments were carried out in triplicate.

The proposed drug release mechanism from constructs (based on the intrinsic nature of PVP and PCL) was assumed to be diffusive in nature [16]. In order to validate this assertion, *in vitro* drug release data (from constructs without AMF application) were fitted to Korsmeyer-Peppas and Higuchi models. For this constructs F1-F4 were selected. The Korsmeyer-Peppas model is normally applied to analyze drug release when the mechanism is not clear. In contrast, the Higuchi model is conventionally used to confirm diffusive drug release from a polymer matrix system. The Korsmeyer-Peppas model is expressed as shown in Eq. (1):

$$\frac{M_t}{M_\infty} = kt^n \quad (1)$$

Here,  $M_t$  is the accumulative quantity of drug released at time  $t$ , and  $M_\infty$  represents the initial drug loading ( $M_t/M_\infty$  represents the fraction drug released at time  $t$ ),  $k$  is a constant characteristic and  $n$  is the release exponent which indicates the release mechanism [25]. The Higuchi model is presented as shown in Eq. (2):

$$M_t = k_H t^{\frac{1}{2}} \quad (2)$$

Here,  $M_t$  is the quantity of cumulative drug release after time  $t$  and  $k_H$  is the Higuchi constant [26].

## 2.6 Antimicrobial activity, cell culture and morphology

Construct antimicrobial activity was investigated using *E. coli* as the test microorganism over a 24 h incubation period. Selected construct samples (as discs *ca.* 10 mm) were assessed. Construct biocompatibility was investigated through cell proliferation and morphology. Human umbilical vein endothelial cells (HUVEC) were

selected, and were provided by American Type Culture Collection (ATCC). Firstly, HUVEC were cultured in Dulbecco's modified eagle's medium with 1% antibiotic and antimycotic solutions (DMEM, high glucose; Gibco, USA), supplied with 10% fetal bovine serum (FBS, Gibco, USA) in 6 cm diameter cell culture dishes at 37°C in humidified atmosphere of 5% CO<sub>2</sub>. The culture medium was changed every 2 days. The samples were fixed with stainless steel rings in the culture dishes [27]. The samples were disinfected by soaking in ethanol for 1 h followed by washing with PBS (three times). Samples were then soaked overnight in cell culture medium before seeding with cells.

HUVEC were seeded on two types of construct samples at a density of  $1.0 \times 10^5$  cells/cm<sup>2</sup>. After 1 and 4 days cell culture, cell morphology was determined following a previously reported method [27]. Fluorescent imaging was used to visualize cell growth and morphology on construct samples. Briefly, HUVEC cultured on samples were fixed using 4% (v/v) formalin (20 min), and were then washed three times using PBS. Cells were then permeabilized using 0.1% Triton X-100 in PBS for 5 min. After washing with PBS, cell cytoskeleton and nuclei were stained with Alexar Fluor 546 phalloidin (Yeasen Biology Technology Co., LTD, China) (1:100 dilution) and 4',6'-diamidino-2-phenylindole hydrochloride (DAPI, Yeasen Biology Technology Co., LTD, China) for 20 min and 5 min, respectively. Samples were then washed three times (PBS) after each staining. Subsequently, cells were visualized using an inverted fluorescent microscope (Nikon, Eclipse Ti-S, Japan).

### 3. Results and discussion

#### 3.1 Fabrication of complex constructs

Fig. 1 shows a schematic diagram of the EHD-hybrid engineering platform utilized in this study. In order to facilitate side-by-side co-engineering function the ES and EHD continuous jetting were setup adjacently on to a programmable X-Y-Z motion stage, providing controlled movement in three dimensions. Four types of polymeric components (F1, F2, F3, and F4) were designed and engineered, through ES, EHD continuous jetting or a combination. Where EHD continuous jetting was used, the projected deposition pathway was uploaded onto the program controller. A detailed description of these structures is provided in Table 1(a).

Fig. 2 shows optical and electron micrographs of random electrospun fibers and aligned 3D printed fibers generated using hybrid technology. Fig. 2(a) shows random fibrous PVP membranes incorporating antibiotic TE-HCL and  $\text{Fe}_3\text{O}_4$  NPs (F1), while Fig. 2(b) presents patterned 3D PCL grids also hosting identical active and functional materials (comprised of horizontal and vertical filaments; stacked ten times to form a square pattern possessing uniform void spacing of  $500\ \mu\text{m}$ , F2). A complex construct comprising PCL printed structures and fibrous PVP membrane (F3) is shown in Fig. 2(c), while multiple intercalation with aligned–random–aligned configuration is shown (F4) in Fig. 2(d). Electron micrographs show random PVP and patterned PCL fibers possess smooth and near uniform diameters (respective of their individual forming method) when prepared using the hybrid platform (Fig. 2(a1)-2(d1)). The inset in Fig. 2(d1) shows formulation F4 at high magnification, in which PVP fibers are clearly

observable. Fig. 2(d) indicates the hybrid engineering platform developed in this study could be used to fabricate constructs with various geometries. Aligned 3D PCL foundation component fibers were near uniform with a mean diameter of 25  $\mu\text{m}$ . Randomly orientated PVP fibers show a reduced mean diameter ( $\sim 1 \mu\text{m}$ ) when compared to printed architectures. This difference is attributed to enhanced drying time arising from the increased deposition distance along with ES instabilities; which expedite solvent evaporation and fiber shrinkage during forming.

In order to further demonstrate structure generation and geometrical complexity and arising from EHD-hybrid engineering, five construct types (P1-P5) were fabricated using the integrative apparatus (detailed descriptions are shown in Table 1(b)). All constructs comprised two components; a 3D patterned structure enforcing platform and a superficial non-ordered topping membrane. The first geometry (P1) possesses PCL fibers arranged in well intercalated horizontal and vertical stacks; with alternating layers for 10 repetitions (void size  $\sim 500 \mu\text{m}$ ). The overall construct is then completed with a fibrous PVP membrane loaded with TE-HCL antibiotic. The second geometry (P2) comprises PCL filaments stacked in the X axis for ten repetitions followed by a further ten stacks in the Y axis. For P2 the void size was maintained at  $\sim 500 \mu\text{m}$  and an identical PVP fibrous membrane was fabricated to blanket the printed architecture. Geometry P3 comprised horizontal and angled filaments with alternating layering for ten repetitions giving rise to parallelogram grid voids (interior angle  $45^\circ$ , length  $\sim 500 \mu\text{m}$ ). As deployed previously, TE-HCL loaded fibrous PVP membranes were used to complete construct engineering. The penultimate geometry, P4, was identical to P1,

however, in this instance 3D patterned PCL filaments were prepared to host Fe<sub>3</sub>O<sub>4</sub> NPs. The last geometry (P5) was an extension to P4; with PVP membranes also encapsulating Fe<sub>3</sub>O<sub>4</sub> NPs (in addition to TE-HCL).

Fig. 3(a)-(e) show optical micrograph plan views of constructs P1 to P5. Both patterned foundation and random superficial layers are observed. Fig. 3(a1)-(e2) show electron micrographs of constructs P1-P5 observed from plan and inclined views. In accordance with the optical data, electron micrographs present similar PCL grid patterned foundations blanketed with a fibrous PVP membrane. Interestingly, a brighter contrast intensity is apparent for 3D PCL 'square' foundation grids. This is attributed to PCL stack fiber height that becomes compromised for angular patterns, leading to a difference in contrast, as shown in Fig. 3(a1)-3(e1).

Fig. 3(a2)-3(e2) show filamentous 3D PCL patterns with near uniform diameters and smooth surface morphology. For P1, P4 and P5 constructs; alternating horizontal and vertical fiber deposition was achieved at an angle of 90° (Fig. 3(a2), (d2) and (e2), respectively). For construct P2, the PCL foundation platform comprised ten stacked horizontal filaments followed by ten stacked vertical structures with excellent accuracy and precision as shown in Fig. 3(b2) with a neat parallelogram void shown further for P4 in Fig. 3(c2).

### *3.2 Fourier transform infra-red spectroscopy*

Fourier Transform Infrared Spectroscopy (FTIR) was used to determine chemical composition of constructs using the 4000-450 cm<sup>-1</sup> region. FTIR spectra of pure

materials and engineered constructs reveal sample composition, as shown in Fig. 4(a) & (b). The presence of PVP polymer was confirmed by absorbance at 1018 and 1290  $\text{cm}^{-1}$ , which are assigned to C-N stretching. Characteristic absorption bands at 2358 and 2954  $\text{cm}^{-1}$  belong to stretching vibrations of C-H. Another characteristic peak attributed to stretching vibrations is found at 1496  $\text{cm}^{-1}$  and is attributed to C=O [12]. PCL polymer produces a strong carbonyl (C=O) peak at 1729  $\text{cm}^{-1}$  and other absorptions between 2868 and 2949  $\text{cm}^{-1}$  arising from methylene ( $\text{CH}_2$ ) groups [15], Similar bands are observed in spectra for constructs P1-P5 shown in Fig. 4(b). A characteristic band of  $\text{Fe}_3\text{O}_4$  is observed at 580  $\text{cm}^{-1}$  and is attributed to the Fe-O bond [17], which can be observed in both constructs P4 and P5 as shown in Fig. 4(b). Characteristic absorption peaks for TE-HCL are observed at 1246  $\text{cm}^{-1}$  (C-N), 1288  $\text{cm}^{-1}$  (C-H stretching vibration) and 1460  $\text{cm}^{-1}$  (O-H stretching vibration) for all spectra of constructs hosting the antibiotic [12], as shown in Fig. 4(b). FTIR spectroscopy indicated PVP, PCL and  $\text{Fe}_3\text{O}_4$  NPs construct components remain stable during EHD.

### *3.3 Mechanical Properties*

Numerous studies have shown mechanical property enhancement of electrospun membranes upon inclusion of metallic nanoparticles [28, 29]. In this study, construct mechanical properties were also improved through addition of nanoparticles. Furthermore, base PCL patterned geometry and design also provided a route to enhance such features.

Mechanical properties of constructs F1-F4 were investigated as shown in Fig. 4(c). Randomly orientated PVP fibers (F1) displayed poor tensile stress ( $< 0.2$  MPa), which is in agreement with a previous report[30]. Aligned PCL foundations for construct F2 displayed a maximum tensile stress of  $>0.4$  MPa. However, the tensile stress of F3 (angular patterning) was lower than F2, but exhibited an increase in tensile strain. Moreover, construct F4 possessed the minimum tensile stress and the maximum tensile strain. This is attributed to a lack of patterned PCL foundation and therefore interlocking. Two breaking points are observed; PVP membrane fracture followed by the breakage of patterned PCL foundation. Mechanical properties of PCL construct components appear appreciably greater than PVP constituents, as the PCL breaking process was more prolonged compared to PVP.

Stress-strain curves for constructs P1-P5, comprising various 3D print-patterned PCL filaments, are shown in Fig. 4(d). A similar two stage breaking process is observed irrespective of construct type. Construct P1 exhibits a maximum tensile stress of 0.3 MPa with the greatest tensile strain of 147%. However, the tensile stress for construct P2 decreased to 0.26 MPa with a minimum tensile strain of 53.6%. This is due to differences in fiber stacking and repetition; since construct P2 possessed reduced intercalation (ten fibers were stacked in one axis for P2, whereas those in P1 were intercalated on a layer-by-layer basis). This indicates fiber printing and intercalating sequence through multi-axial layering impacts the overall constructs mechanical properties. Construct P3 comprised parallelogram shaped voids ( $45^\circ$ ), which would enable greater flexibility. Thus, its maximum tensile stress was  $\sim 0.5$  MPa with the



maximum tensile strain close to 500%. The greatest tensile stress for construct P4 was 0.7 MPa, although it possessed a breaking tensile strain of ~362%, with the difference between P1 and P4 being inclusion of magnetic NPs (P4). The results coincide with a previous report citing well dispersed Fe<sub>3</sub>O<sub>4</sub> NPs improve mechanical properties of fibrous systems[31]. Construct P5 displayed best mechanical properties; with a maximum tensile stress of >1.2 MP and the greatest tensile strain (~659%). For this construct, NPs were also incorporated in to the superficial PVP membrane. Therefore, construct design parameters such as printing sequence, direction, angle and additive inclusion provide routes to modulate mechanical properties of hybrid drug delivery systems.

#### *3.4 Construct hydrophilicity*

Biomaterial contact angle has significant impact on drug release from a device [16] and the materials surface is the first point of interaction with biological (host) surroundings. Thus, wettability is influenced primarily by surface characteristics which in turn impacts bio-interface behaviour [32, 33]. In addition, wettability has also been shown to modulate hydrophobicity, which is an important parameter in drug release from a delivery system [34]. Therefore, the constructs produced in this study incorporate both hydrophilic (PVP) and hydrophobic (PCL) fibers, making it a potential active carrier delivery system for controlled and sustained drug release. Device hydrophilicity was determined by measuring direct contact angles (CAs) between a PBS droplet (1uL, pH 7.4) and the constructs surface. Initial CA and its gradual change at pre-determined time

intervals on constructs F1-F4 and P1-P5 were measured, as shown in Fig. 5. The initial PBS CA on construct surface are presented in Fig. 5(a) and 5(c), respectively. Fig. 5(b) and 5(d) are magnified digital images of droplet behaviour on EHD-hybrid engineered construct surfaces at 0, 100 and 300 s. The initial CA for F1 was  $39^\circ$ , which subsequently reduced to  $\sim 0^\circ$  after 100s. This is due to the highly hydrophilic nature of PVP polymer, which dissolved spontaneously in PBS [35]. CAs of constructs F2, F3 and F4 were near identical  $\sim 70^\circ$  (at 0 sec). After 300s the CA of F3 was  $\sim 0^\circ$ . The overcoat membrane for both constructs is most likely to be the driving factor for these values. However, constructs F2 and F4 show similar CAs over 0-100s. This is due to PCL stability and resistance to rapid PBS degradation. Previous findings report PCL fibers to exhibit deionized water CAs of  $\sim 110^\circ$  [36], which suggests test medium, void space and porosity change could all impact CA behavior.

Constructs P1-P5 possess fibrous PVP layering. However, differences in CA were observed which are attributed to the aligned PCL foundations. The CA of construct P1 was  $40^\circ$ , which is near identical to construct F1. However, altering PCL foundation geometry to stacked, with parallelogram void structure or made to host  $\text{Fe}_3\text{O}_4$  NPs within foundations reduces device hydrophilicity, which is identical to construct F2 (PCL foundation loaded with TE-HCL and  $\text{Fe}_3\text{O}_4$  NPs). CAs of constructs P1-P5 decreased with time, due to dissolution of PVP membranes. According to the results, coupling EHD continuous jetting PCL foundations with PVP membranes enhances the CAs. Furthermore, as described earlier, the difference in sample contrast (shown in Fig.

3(a1)-(e1)), which arises due to change in micro-structure height may also be responsible for variations to CAs. However, all construct CAs were below 90°, indicating their hydrophilic nature with good wettability. Thus, constructs fulfilled moisture integration requirements that is crucial for active interaction at the bio-interface.

### *3.5 In vitro TE-HCL release studies*

TE-HCL release behaviours from constructs was investigated in PBS (pH 7.4, triplicate) at the ambient temperature (25°C). TE-HCL release from fundamental constructs F1- F4 were investigated with and without an external AMF, as shown in Fig. 6(a). It could be observed that with the aid of an AMF trigger, TE-HCL release was expedited. PVP membranes dissolved rapidly in PBS, causing TE-HCL release from construct F1 reaching 96% at 600 min with an AMF, with the non-triggered construct releasing over 75% of the antibiotic. However, TE-HCL release from construct F2 was retarded up to 60 min, and reached 20% at 600 min without AMF application. The slow and prolonged release of TE-HCL from construct F2 is due to the hydrophobic nature of PCL. TE-HCL release reached only 40% at 600 min for construct F2, but was enhanced upon application of AMF, which is far less when compared to other constructs. For TE-HCL release from co-polymer systems comprising aligned PCL foundations and a PVP membrane (F3 and F4), a rapid release of TE-HCL was followed by a long period of sustained release, indicating a two-tier mechanism. Comparing construct F3 to F4, the latter displayed a much lower and prolonged active

release rate that was due to increased PCL quantities in the overall composition (PCL-PVP-PCL). The release behaviour of TE-HCL from constructs P1-P5 are shown in Fig. 6(b). TE-HCL was only incorporated in PVP membranes for constructs P1-P5. Constructs P4 and P5 are identical to P1, except for Fe<sub>3</sub>O<sub>4</sub> NPs incorporation into P4 and P5. Due to the highly hydrophilic nature of PVP polymer, all TE-HCL release profiles were near complete at 30 min, and constructs P1-P3 exhibit rapid active release during the first 3 min followed by sustained release over the next 18 min. However, it was found that appreciable variations in TE-HCL release behaviour from patterned PCL platforms is clear. Modification of PCL foundation pattern on the PVP membrane accelerated TE-HCL release. At 3 minutes, the releases of TE-HCL from constructs P1-P3 reached ~90%. This initial rapid release is attributed to TE-HCL drug distribution near or embedded in the surface of the PVP membrane of constructs. Over the 21 min' assessment period, constructs P1-P3 all released 100% TE-HCL. However, release of TE-HCL from pure PVP fiber membrane was ~77.6%, indicating an impact on the initial burst release phase. Previous studies have shown that modification to a scaffold like structure (or a 3D matrix) is a viable approach to control drug release [37]. The rapid release of TE-HCL from PVP matrix clearly suggests potential applications where rapid action is required. TE-HCL release from constructs P4 and P5 also present a similar trend, although drug release was further investigated using AMF. Triggered drug release from constructs P4-P5 (both loaded with 0.5 % w/w Fe<sub>3</sub>O<sub>4</sub> NPs and 0.5% TE-HCL) was assessed over a similar assessment release period. The introduction of AMF (~40 KHz) around NP embedded constructs induced greater drug release

compared to the non-treated sample (P1). The release of TE-HCL from constructs P4 and P5 reached 100% within the first 2 min. This is due to intensified motion of molecules within NP embedded constructs (P4 and P5) with actuated activity of Fe<sub>3</sub>O<sub>4</sub> NPs upon exposure to AMF. Drug release profiles indicate AMF could be used to accelerate active release and geometry of PCL foundations has a clear influence on the rate of drug release.

Drug release data for constructs F1-F4 were fitted to Korsmeyer-Peppas and Higuchi models. For Korsmeyer-Peppas model; regression coefficients and  $n$  values were calculated (Table 2). For F1, F2, F3 and F4 constructs;  $n$  values were 0.0858, 0.4792, 0.0735 and 0.0668, respectively. Here, for  $n < 0.45$  Fickian diffusion is most likely, while for  $0.45 < n < 0.89$ , an anomalous transport process is suggested, which involves various factors; demanding at least two parameters to clarify diffusion and relaxation behavior for non-Fickian diffusion [16, 25, 38]. Based on  $n$  values the drug release mechanism from F2 (pure PCL fibers) appears to follow non-Fickian diffusion. As  $n < 0.45$  was established for constructs F1, F3 and F4, Fickian diffusion dominates the drug release process. For Higuchi model, if the cumulative drug release content is linearly dependent on square root of time, drug release is likely to be diffusion-controlled [39]. Drug release data with corresponding parameters is displayed in Table 2. The high  $R^2$  values suggests that drug release from all complicated constructs is *via* diffusion mechanism. While both models are in agreement for release mechanisms related to constructs F1, F3 and F4; construct F2 could actually be classed to display Quasi-Fickian diffusion as demonstrated in previous studies since  $n$  is below 0.5 [40].

Fig. 6(c) shows an electron micrograph of construct F1 during the TE-HCL *in vitro* release study removed at 20s. PVP fibers had lost their integrity and appeared as shard structures. Fig. 6(d) shows an electron micrograph of construct F2 removed from the *in vitro* study at 600 min. PCL fibers also become less well-defined with irregular and swollen topographical features due to interaction and uptake of the release medium *via* diffusion. However, it could be seen that TE-HCL encapsulated in both PVP membrane and PCL patterned foundations (in a single device) could deliver a two-tier active release strategy. Furthermore, Fe<sub>3</sub>O<sub>4</sub> NPs have the potential to enhance TE-HCL release. Thus, considering aforementioned release mechanisms, together with Fe<sub>3</sub>O<sub>4</sub> NP induced effects, bespoke construct engineering using functional materials, geometrical features and polymer variations provide multi-modal therapy potential.

### *3.6 Antimicrobial activity and biological evaluation of constructs*

Construct antimicrobial activity was investigated using *E.coli* as the test microorganism. Constructs were prepared using PCL patterned foundations loaded with TE-HCL. Constructs F2 and F3 were selected for assessment. Fig. 7(a-c) show disc samples to form inhibition zones at 16, 20 and 24 h incubation. The inhibition zones appear stable during this period. However, inhibition zone diameter for disc F3 was significantly wider than both F2 and the PCL foundation (loaded with TE-HCL only) as shown in Fig. 7(d). This could be due attributed to PVP membrane overcoat hosting TE-HCL and Fe<sub>3</sub>O<sub>4</sub> NPs. Inhibition zones for disc F2 were lower than PCL foundations,

indicating Fe<sub>3</sub>O<sub>4</sub> NPs could also reduce antimicrobial activity. The three construct discs display clear inhibition zones, indicating antimicrobial function.

Although both PCL and PVP are FDA approved materials, multi-material constructs still pose potential toxic risks to cells due to residual solvent, process induced changes and environmental impact. Hence, a biological assay was performed to evaluate cytotoxicity of constructs F2 and F3. Due to PVP hydrophilicity, the polymer was blended with PCL and TE-HCL, and the system was used as the modified covering membrane for construct F3. The PCL foundation was identical to foundations devised for specimen F2. Cell behavior on construct F2 and F3 was observed using fluorescent microscopy over a four day cell culture period. Fig. 7(e1)-(f4) show micrographs obtained from fluorescent microscopy. HUVEC were stained red for F-actin and blue for cell nuclei. After incubation for four days, both constructs F2 (Fig. 7(e1)-(e4)) and F3 (Fig. 7(f1)-(f4)) showed biocompatibility. A large number of cells were on the samples, especially for patterned PCL foundations (Fig. 7(e1)-(e4)), HUVEC accumulated on aligned PCL filaments assuming the shape of grids as shown in micrographs. However, during the incubation period, cell proliferation and growth was observed for constructs F2 and F3. Cell morphology appeared spindled, suggesting cell growth on both components. Therefore, these results confirm complex construct biocompatibility, engineered using EHD-hybrid technologies.

#### **4. Conclusions**

In summary, complex constructs comprising patterned PCL foundations and electrospun PVP membranes were successfully fabricated using a hybrid EHD apparatus; merging ES and EHD continuous jetting. Results show structure complexity through geometrical variation, material selection and co-engineering platform. The presence of various components was confirmed using FTIR. Alteration to the printed base PCL foundation influenced PBS contact angle, mechanical properties and TE-HCL release profiles. Classical burst release of TE-HCL was observed from constructs, which could be tailored through PCL foundation geometry. Furthermore, two-tier drug release was achieved based on PCL foundation (sustained) and PVP coating membrane (rapid). For the sustained release, AMF trigger provided a route to expedite antibiotic release. All constructs exhibited antibacterial activity and good cell biocompatibility. The findings indicate potential value for hybrid engineering and novel multi-stage therapies.

### **Acknowledgements**

This work was financially supported by the National Nature Science Foundation of China (No. 81771960), the Fundamental Research Funds for the Central Universities (2017QNA5017) and Key Technologies R&D Program of Zhejiang Province (2015C02035).

### **References**



- [1] K.E. Uhrich, S.M. Cannizzaro, R.S. Langer, K.M. Shakesheff, Polymeric systems for controlled drug release, *Chem. Rev.* 99 (1999) 3181-3198.
- [2] J. Jia, C.X. Wang, K.L. Chen, Y.J. Yin, Drug release of yolk/shell microcapsule controlled by pH-responsive yolk swelling, *Chem. Eng. J.* 327 (2017) 953-961.
- [3] A. Tamayo, M.A. Mazo, R. Ruiz-Caro, A. Martin-Illana, L.M. Bedoya, M.D. Veiga-Ochoa, J. Rubio, Mesoporous silicon oxycarbide materials for controlled drug delivery systems, *Chem. Eng. J.* 280 (2015) 165-174.
- [4] L. Wang, M.W. Chang, Z. Ahmad, H.X. Zheng, J.S. Li, Mass and controlled fabrication of aligned PVP fibers for matrix type antibiotic drug delivery systems, *Chem. Eng. J.* 307 (2017) 661-669.
- [5] L.Y. Huang, C. Branford-White, X.X. Shen, D.G. Yu, L.M. Zhu, Time-engineered biphasic drug release by electrospun nanofiber meshes, *Int. J. Pharm.* 436 (2012) 88-96.
- [6] T.S. Anirudhan, P.L. Divya, J. Nima, Synthesis and characterization of novel drug delivery system using modified chitosan based hydrogel grafted with cyclodextrin, *Chem. Eng. J.* 284 (2016) 1259-1269.
- [7] A. Xiang, A.J. Mchugh, Quantifying sustained release kinetics from a polymer matrix including burst effects, *J. Membr. Sci.* 371 (2011) 211-218.
- [8] T.J. Sill, H.A. von Recum, Electrospinning: Applications in drug delivery and tissue engineering, *Biomaterials.* 29 (2008) 1989-2006.

- [9] X.L. Hu, S. Liu, G.Y. Zhou, Y.B. Huang, Z.G. Xie, X.B. Jing, Electrospinning of polymeric nanofibers for drug delivery applications, *J. Control. Release.* 185 (2014) 12-21.
- [10] J.U. Park, J.H. Lee, U. Paik, Y. Lu, J.A. Rogers, Nanoscale Patterns of Oligonucleotides Formed by Electrohydrodynamic Jet Printing with Applications in Biosensing and Nanomaterials Assembly, *Nano. Lett.* 8 (2008) 4210-4216.
- [11] M. Ignatova, N. Manolova, I. Rashkov, Electrospinning of poly(vinyl pyrrolidone)-iodine complex and poly(ethylene oxide)/poly(vinyl pyrrolidone)-iodine complex – a prospective route to antimicrobial wound dressing materials, *Eur. Polym. J.* 43 (2007) 1609-1623.
- [12] J.-C. Wang, M.-W. Chang, Z. Ahmad, J.-S. Li, Fabrication of patterned polymer-antibiotic composite fibers via electrohydrodynamic (EHD) printing, *J. Drug. Deliv. Sci.Tec.* 35 (2016) 114-123.
- [13] E. Schlesinger, N. Ciaccio, T.A. Desai, Polycaprolactone thin-film drug delivery systems: Empirical and predictive models for device design, *Mater. Sci. Eng. C-Mater. Biol. Appl.* 57 (2015) 232-239.
- [14] D. Yang, B. Lu, Y. Zhao, X. Jiang, Fabrication of Aligned Fibrous Arrays by Magnetic Electrospinning, *Adv. Mater.* 19 (2007) 3702-3706.
- [15] B.L. Wang, H.X. Zheng, M.W. Chang, Z. Ahmad, J.S. Li, Hollow polycaprolactone composite fibers for controlled magnetic responsive antifungal drug release, *Colloids Surf., B.* 145 (2016) 757-767.

- [16] Y. Gao, M.W. Chang, Z. Ahmad, J.S. Li, Magnetic-responsive microparticles with customized porosity for drug delivery, *Rsc. Adv.* 6 (2016) 88157-88167.
- [17] S. Sadighian, K. Rostamizadeh, H. Hosseini-Monfared, M. Hamidi, Doxorubicin-conjugated core-shell magnetite nanoparticles as dual-targeting carriers for anticancer drug delivery, *Colloids. Surf., B.* 117 (2014) 406-413.
- [18] K. Niikura, N. Iyo, Y. Matsuo, H. Mitomo, K. Ijio, Sub-100 nm Gold Nanoparticle Vesicles as a Drug Delivery Carrier enabling Rapid Drug Release upon Light Irradiation, *Acs. Appl. Mater. Inter.* 5 (2013) 3900-3907.
- [19] C. Maderuelo, A. Zarzuelo, J.M. Lanao, Critical factors in the release of drugs from sustained release hydrophilic matrices, *J. Control. Release.* 154 (2011) 2-19.
- [20] A. Kuksal, A.K. Tiwary, N.K. Jain, S. Jain, Formulation and in vitro, in vivo evaluation of extended-release matrix tablet of zidovudine: Influence of combination of hydrophilic and hydrophobic matrix formers, *Aaps. Pharmscitech.* 7 (2006) 9.
- [21] P. Karuppuswamy, J.R. Venugopal, B. Navaneethan, A.L. Laiva, S. Ramakrishna, Polycaprolactone nanofibers for the controlled release of tetracycline hydrochloride, *Mater. Lett.* 141 (2015) 180-186.
- [22] R.N. Sindhura, S. Sowmya, J.D. Bumgardner, K.P. Chennazhi, R. Biswas, R. Jayakumar, Tetracycline nanoparticles loaded calcium sulfate composite beads for periodontal management, *BBA-Gen. Subjects.* 1840 (2014) 2080-2090.

- [23] M.E. El-Naggar, A.M. Abdelgawad, C. Salas, O.J. Rojas, Curdlan in fibers as carriers of tetracycline hydrochloride: Controlled release and antibacterial activity, *Carbohydr. Polym.* 154 (2016) 194-203.
- [24] P. Askari, P. Zahedi, I. Rezaeian, Three-layered electrospun PVA/PCL/PVA nanofibrous mats containing tetracycline hydrochloride and phenytoin sodium: A case study on sustained control release, antibacterial, and cell culture properties, *J. Appl. Polym. Sci.* 133 (2016) 43309.
- [25] M.A. Zarandi, P. Zahedi, I. Rezaeian, A. Salehpour, M. Gholami, B. Motealleh, Drug release, cell adhesion and wound healing evaluations of electrospun carboxymethyl chitosan/polyethylene oxide nanofibres containing phenytoin sodium and vitamin C, *Iet Nanobiotechnology.* 9 (2015) 191-200.
- [26] J. Siepmann, N.A. Peppas, Higuchi equation: Derivation, applications, use and misuse, *Int. J. Pharmaceut.* 418 (2011) 6-12.
- [27] D. Li, W. Tong, N. He, W. Jing, W. Chen, L. He, H. Chen, H.A. Ei-Hamshary, S.S. Al-Deyab, Q. Ke, Three-dimensional polycaprolactone scaffold via needleless electrospinning promotes cell proliferation and infiltration, *Colloids. Surf. B.* 121 (2014) 432.
- [28] C.W. Chou, S.H. Hsu, H. Chang, S.M. Tseng, H.R. Lin, Enhanced thermal and mechanical properties and biostability of polyurethane containing silver nanoparticles, *Polym. Degrad. Stab.* 91 (2006) 1017-1024.
- [29] F.A. Sheikh, N.A.M. Barakat, M.A. Kanjwal, A.A. Chaudhari, I.H. Jung, J.H. Lee, H.Y. Kim, Electrospun antimicrobial polyurethane nanofibers containing

- silver nanoparticles for biotechnological applications, *Macromol. Res.* 17 (2009) 688-696.
- [30] S. Baccaro, L.A. Pajewski, G. Scoccia, R. Volpe, J.M. Rosiak, Mechanical properties of polyvinylpyrrolidone (PVP) hydrogels undergoing radiation, *Nucl. Instrum. Meth. B.* 105 (1995) 100-102.
- [31] N. Cai, C. Li, C. Han, X. Luo, L. Shen, Y. Xue, F. Yu, Tailoring mechanical and antibacterial properties of chitosan/gelatin nanofiber membranes with Fe<sub>3</sub>O<sub>4</sub> nanoparticles for potential wound dressing application, *Appl. Surf. Sci.* 369 (2016) 492-500.
- [32] T. Tsukagoshi, Y. Kondo, N. Yoshino, Preparation of thin polymer films with controlled drug release, *Colloids. Surf. B.* 57 (2007) 219-225.
- [33] S.T. Wu, B.L. Wang, Z. Ahmad, J. Huang, M.W. Chang, J.S. Li, Surface modified electrospun porous magnetic hollow fibers using secondary downstream collection solvent contouring, *Mater. Lett.* 204 (2017) 73-76.
- [34] B.L. Wang, M.D. Wang, M.W. Chang, Z. Ahmad, J. Huang, J.S. Li, Non-concentric multi-compartment fibers fabricated using a modified nozzle in single-step electrospinning, *Mater. Lett.* 202 (2017) 134-137.
- [35] S.J. Cho, M.J. Sang, M. Kang, H.S. Shin, H.Y. Ji, Preparation of hydrophilic PCL nanofiber scaffolds via electrospinning of PCL/PVP- b -PCL block copolymers for enhanced cell biocompatibility, *Polymer.* 69 (2015) 95-102.

- [36] T. Rafael Bergamo, Cec, iacute, W. lia Buzatto, Acirc, M. ngela Maria, Electrospun multilayer chitosan scaffolds as potential wound dressings for skin lesions, *Eur. Polym. J.* (2017) 161–170.
- [37] A. Szentivanyi, T. Chakradeo, H. Zernetsch, B. Glasmacher, Electrospun cellular microenvironments: Understanding controlled release and scaffold structure, *Adv. Drug. Deliver. Rev.* 63 (2011) 209-220.
- [38] N.A. Peppas, J.J. Sahlin, A Simple Equation for the Description of Solute Release. III. Coupling of Diffusion and Relaxation, *Int. J. Pharmaceut.* 57 (1989) 169-172.
- [39] E. Aznar, M.D. Marcos, R. Martinez-Manez, F. Sancenon, J. Soto, P. Amoros, C. Guillem, pH- and Photo-Switched Release of Guest Molecules from Mesoporous Silica Supports, *J. Am. Chem. Soc.* 131 (2009) 6833-6843.
- [40] P. Mehta, A.A. Al-Kinani, R. Haj-Ahmad, M.S. Arshad, M.W. Chang, R.G. Alany, Z. Ahmad, Electrically atomised formulations of timolol maleate for direct and on-demand ocular lens coatings, *Eur. J. Pharm. Biopharm.* 119 (2017) 170-184.

## **Table and Figure Captions**

### **Tables**

**Table 1(a).** Detailed descriptions of constructs F1-F4.

**Table 1(b).** Detailed description of constructs P1-P5. The total number of layers for all construct foundations was 20.

**Table 2.** Application of Korsmeyer-Peppas and Higuchi models to drug released from constructs F1-F4.

### **Figures**

**Fig. 1.** Schematic diagram of hybrid EHD apparatus comprising both 3D-printing and electrospinning components. Example of engineered construct (and process) shown in two electron micrographs; firstly as the mechanically supporting aligned PCL fibrous platform and then randomly spun PVP membrane on its surface.

**Fig. 2.** (a)-(d) are Optical micrographs of constructs F1-F4 (scale bar = 500  $\mu\text{m}$ ). (a1) - (d1) show electron micrographs of constructs F1-F4. Insets (a1)-(d1) are high magnifications of constructs F1-F4.

**Fig. 3.** (a)-(e) are optical micrographs of constructs P1-P5 (scale bar = 500  $\mu\text{m}$ ). (a1) - (e1) show electron micrographs of constructs P1-P5 (scale bar = 500  $\mu\text{m}$ ). (a2) - (e2) are inclined electron micrographs of constructs P1-P5 (scale bar = 200  $\mu\text{m}$ ).

**Fig. 4.** (a) FTIR spectra of pure PCL, Fe<sub>3</sub>O<sub>4</sub> NPs, TE-HCL and PVP. (b) FTIR spectra of constructs P1-P5. (c) Stress-strain curves for constructs F1-F4. (d) Stress-strain curves for constructs P1-P5.

**Fig. 5.** (a) and (c) are contact angles for constructs F1-F4 and P1-P5 at 0 s, respectively, upon instant droplet-membrane contact ( $t < 1$  s). (b) and (d) show droplet spreading on constructs at selected time intervals ( $1 < t < 100$  and  $300$  s).

**Fig. 6.** (a) TE-HCL release profiles from constructs F1-4, with and without AMF application. (b) TE-HCL release profiles from constructs P1-5. Error bars indicate mean  $\pm$  standard deviation (sample number  $n=3$ ). (c) Electron micrograph of construct F1 removed at 20s during in vitro release study. (d) Electron micrograph of PCL construct P2 removed at 600 min during in vitro release study.

**Fig. 7.** Inhibition zones for PCL constructs F2 and F3 (incubated with *E. coli*) at (a) 16 (b) 20 and (c) 24h. (d) Inhibition zone diameter at various assessment time points. (e)-(f) are fluorescent micrographs of HUVEC cultured on constructs F2 and F3 (at day 4) showing; (e1 and f1) bright-field micrographs, (e2 and f2) HUVEC cytoskeleton, (e3 and f3) HUVEC nucleus and (e4 and f4) whole HUVEC.

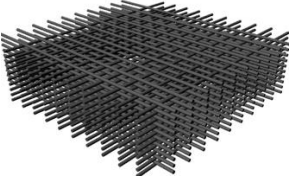
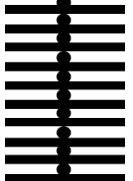
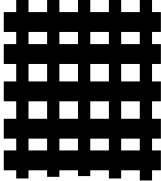
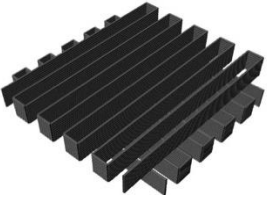
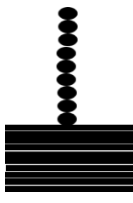
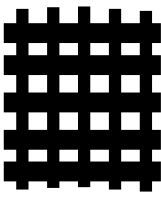
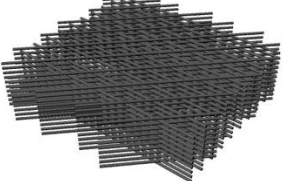
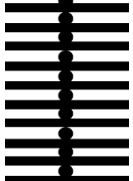
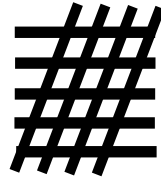
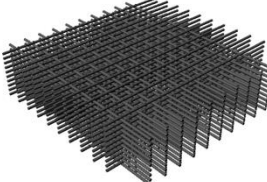
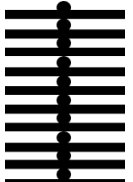
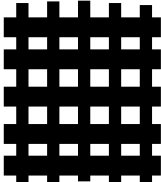
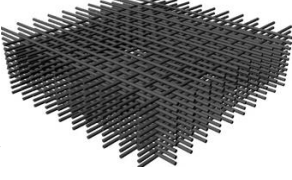
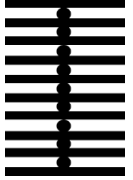
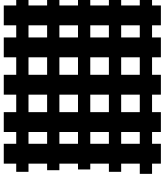


## Tables

**Table 1(a)**

<b>Construct</b>	<b>Fiber integration and features</b>
<b>F1</b>	<b>PVP (random fibers), TE-HCL and Fe<sub>3</sub>O<sub>4</sub></b>
<b>F2</b>	<b>PCL (20 layered fibers), TE-HCL and Fe<sub>3</sub>O<sub>4</sub></b>
<b>F3</b>	<b>F2+F1</b>
<b>F4</b>	<b>F2+F1+F2</b>

Table 1(b)

Structure of foundation			TE-HCL	Fe <sub>3</sub> O <sub>4</sub> NPs
3D constructs	Cross-section view	Top view	Location	Location
P1 			PVP membrane	No Fe <sub>3</sub> O <sub>4</sub> NPs
P2 			PVP membrane	No Fe <sub>3</sub> O <sub>4</sub> NPs
P3 			PVP membrane	No Fe <sub>3</sub> O <sub>4</sub> NPs
P4 			PVP membrane	PCL foundation
P5 			PVP membrane	PVP membrane

**Table 2**

<b>Construct</b>	<b>Model</b>	<b>Equation</b>	<b>n</b>	<b>R<sup>2</sup></b>
<b>F1</b>	Korsmeyer- Pappas	$\text{Log} (M_t/M_\infty \times 100) = 1.7867 + 0.0858 \times \log (t)$	0.0858	0.9797
	Higuchi	$M_t/M_\infty \times 100 = 59.6452 + 4.4864 \times t^{1/2}$	—	0.9574
<b>F2</b>	Korsmeyer- Pappas	$\text{Log} (M_t/M_\infty \times 100) = -0.0097 + 0.4792 \times \log (t)$	0.4792	0.9530
	Higuchi	$M_t/M_\infty \times 100 = 1.4201 + 0.7876 \times t^{1/2}$	—	0.9536
<b>F3</b>	Korsmeyer- Pappas	$\text{Log} (M_t/M_\infty \times 100) = 1.5583 + 0.0735 \times \log (t)$	0.0735	0.9566
	Higuchi	$M_t/M_\infty \times 100 = 45.6095 + 0.5167 \times t^{1/2}$	—	0.9528
<b>F4</b>	Korsmeyer- Pappas	$\text{Log} (M_t/M_\infty \times 100) = 1.4030 + 0.0668 \times \log (t)$	0.0668	0.9872
	Higuchi	$M_t/M_\infty \times 100 = 31.9500 + 0.2753 \times t^{1/2}$	—	0.9563

## Figures

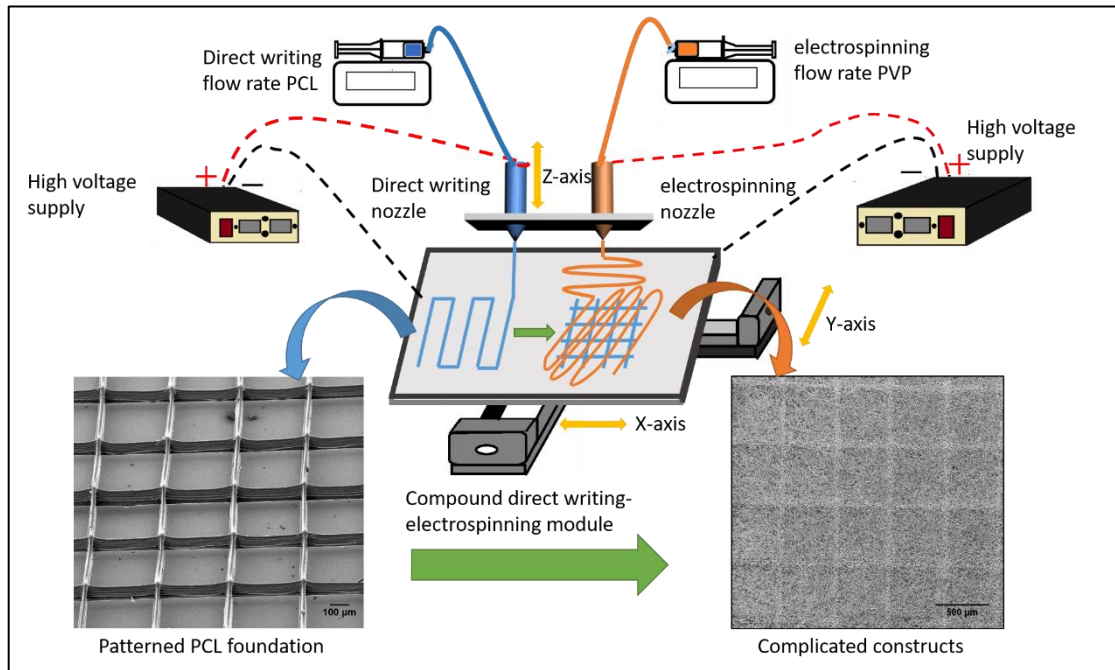


Fig. 1

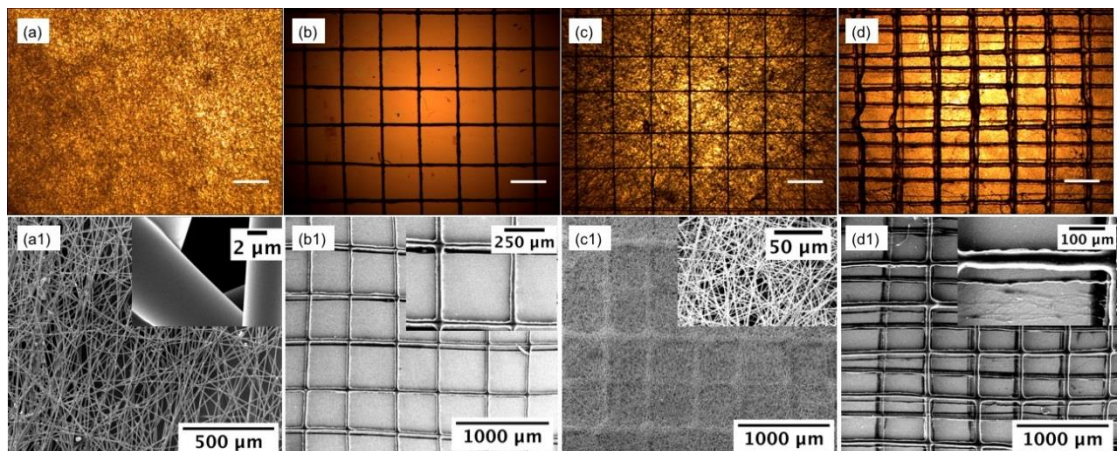


Fig. 2

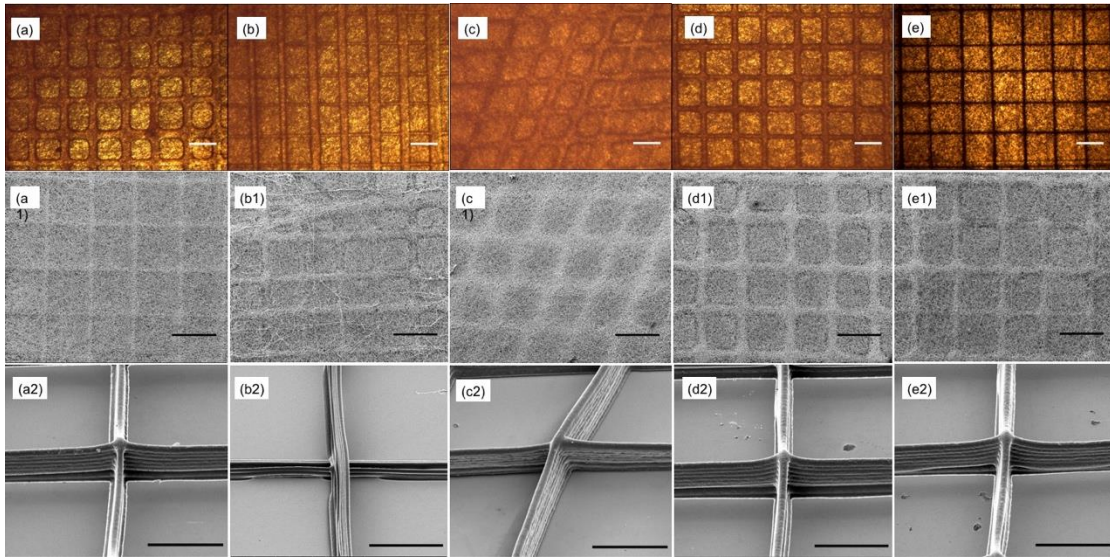
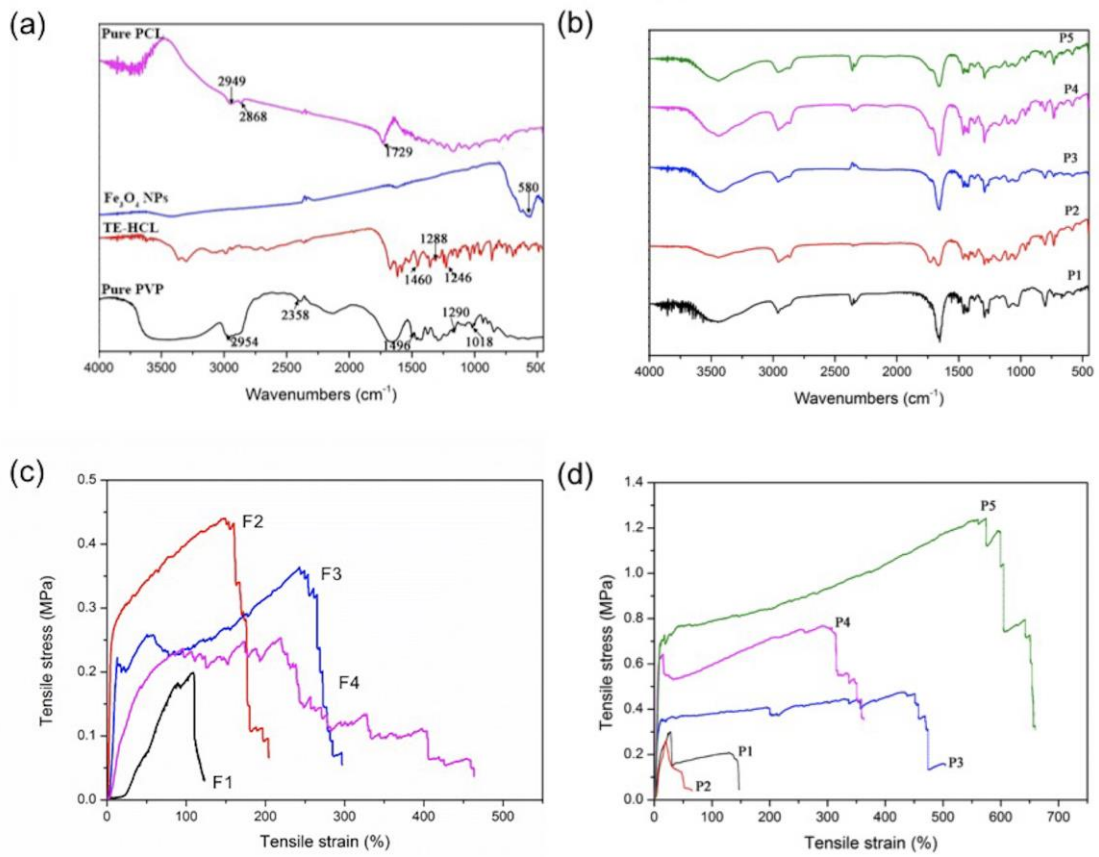
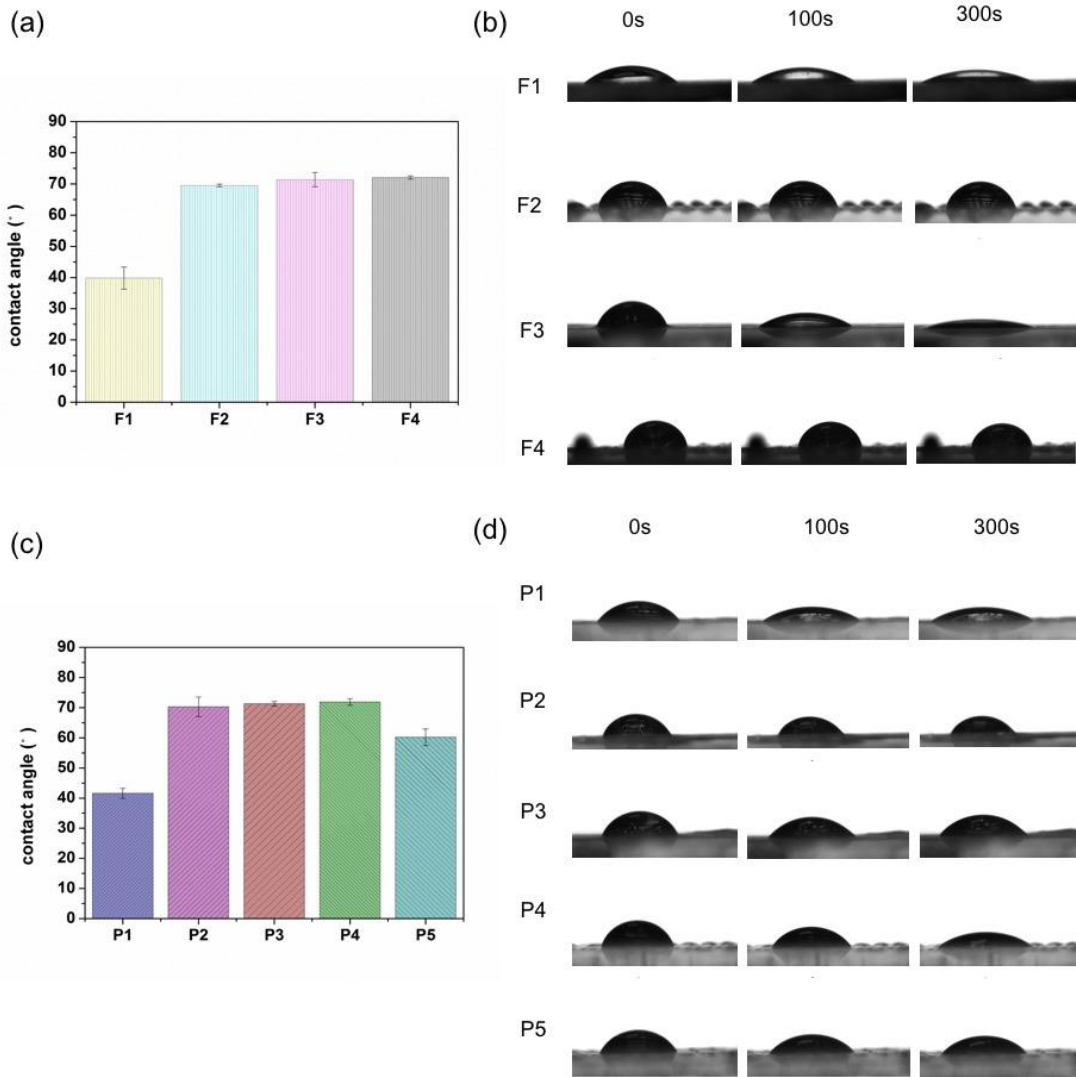


Fig. 3



**Fig. 4**



**Fig. 5**

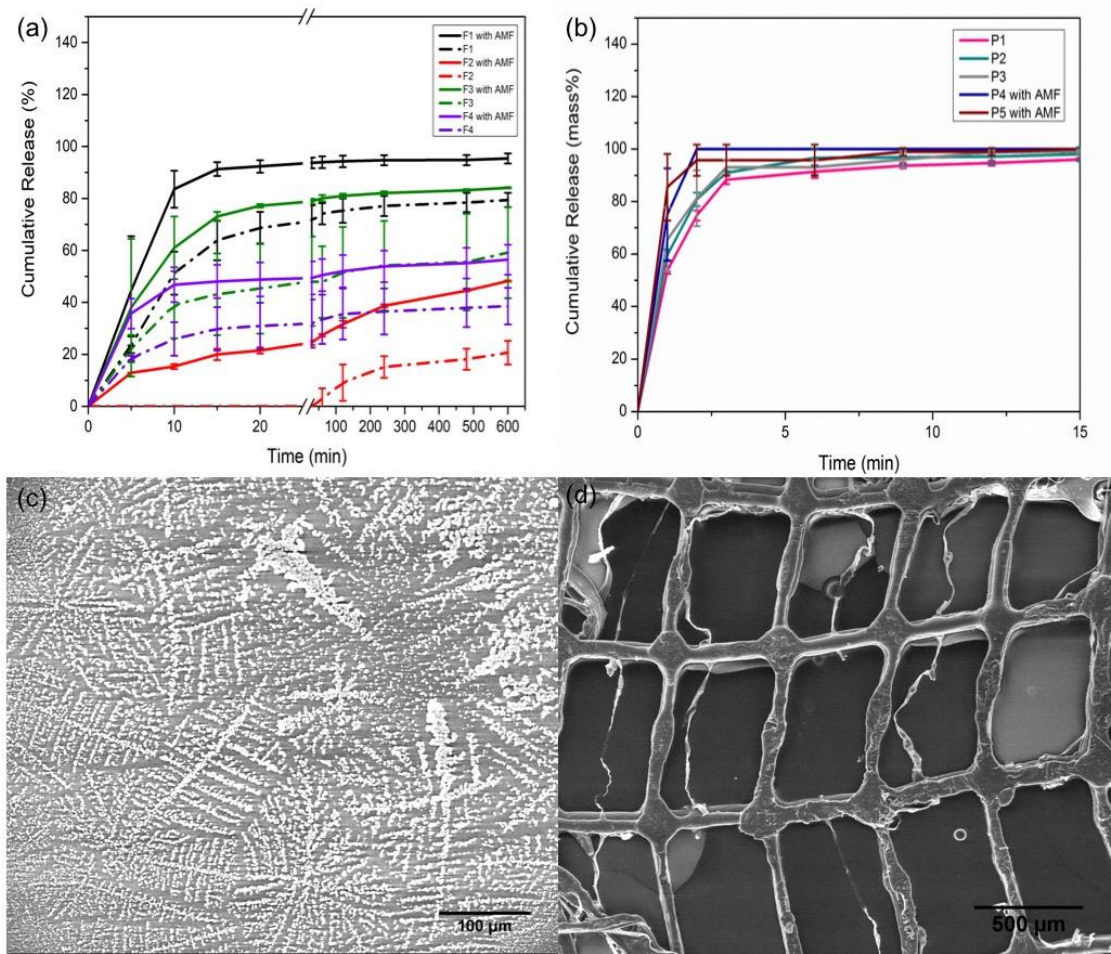
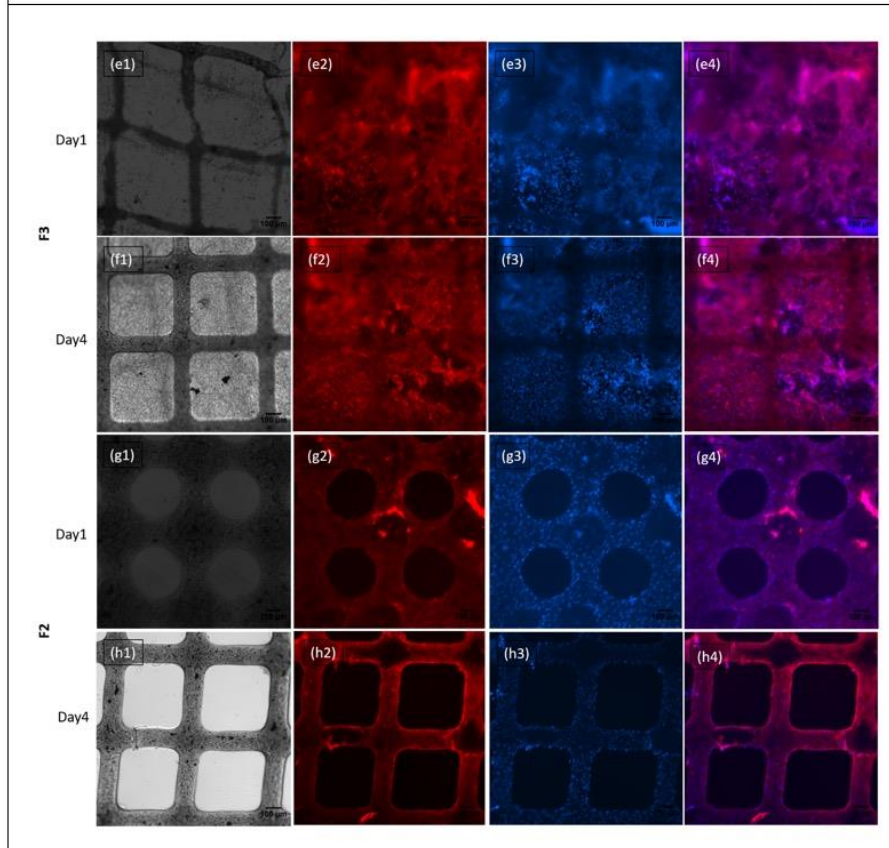
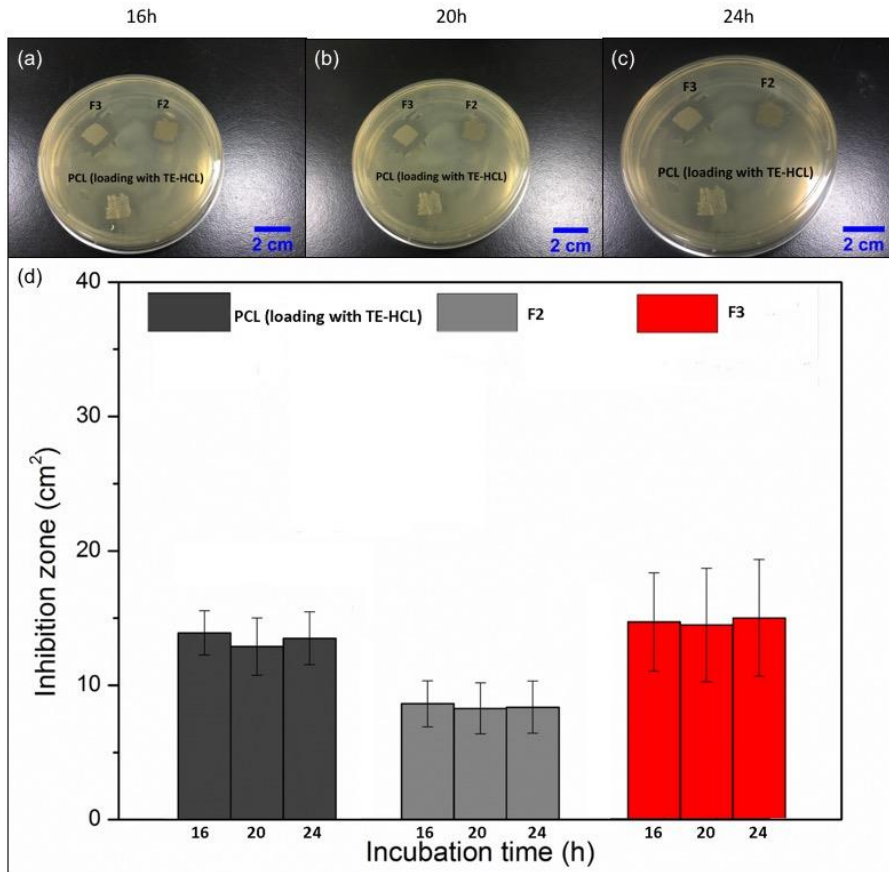


Fig. 6





**Fig. 7**